AGU PUBLICATIONS

Radio Science

RESEARCH ARTICLE
10.1002/2014RS005505

Special Section:
URSI Symposium on Radiowave Propagation and Remote Sensing, 2013

Aquarius: Status and recent results

D. M. Le Vine[1], E. P. Dinnat[1,2], G. S. E. Lagerloef[3], P. de Matthaeis[4], S. Abraham[5], C. Utku[4], and H. Kao[3]

[1]Goddard Space Flight Center, Greenbelt, Maryland, USA, [2]School of Earth and Environmental Sciences, Chapman University, Orange, California, USA, [3]Earth and Space Research, Seattle, Washington, USA, [4]GESTAR, Goddard Space Flight Center, Greenbelt, Maryland, USA, [5]Wyle, Goddard Space Flight Center, Greenbelt, MD

Abstract Aquarius is a combination active/passive instrument at L band designed to map sea surface salinity globally from space. The radiometer (passive) is the primary instrument for retrieving salinity, and the scatterometer (active) provides information to correct for a major source of error, sea surface roughness (waves). In addition, the radiometer includes a number of special features designed to meet the goal for this challenging measurement, including measurement of the third Stokes parameter to help with the correction for Faraday rotation and rapid sampling to help with the mitigation of radio frequency interference. Aquarius was launched on 10 June 2011 aboard the Aquarius/SAC-D observatory and has been working well. The salinity retrieval continues to improve, and the special features suggest the potential for new applications of remote sensing from space at L band.

Key Points:
- Status of the Aquarius instrument and retrieval of sea surface salinity
- Examples of measurements including Faraday rotation, RFI, and salinity retrievals

Correspondence to:
D. M. Le Vine,
david.m.levine@nasa.gov

Citation:
Le Vine, D. M., E. P. Dinnat, G. S. E. Lagerloef, P. de Matthaeis, S. Abraham, C. Utku, and H. Kao (2014), Aquarius: Status and recent results, *Radio Sci.*, *49*, 709–720, doi:10.1002/2014RS005505.

Received 30 APR 2014
Accepted 10 AUG 2014
Accepted article online 13 AUG 2014
Published online 11 SEP 2014

1. Introduction

Aquarius is an L band instrument designed to map the surface salinity field of the global oceans [*Le Vine et al.*, 2007; *Lagerloef et al.*, 2008]. Salinity together with temperature determines ocean water density, and density is important for understanding ocean circulation and its impact on climate [*Lagerloef et al.*, 2008; *Le Vine et al.*, 2010]. Salinity at the surface changes with the balance between evaporation and precipitation; and therefore, the patterns and changes in salinity can also help with understanding the global water cycle.

Aquarius is designed to focus on the open ocean where the science objective is to monitor the seasonal and interannual variations of the large-scale features of the surface salinity field by providing salinity maps on a monthly basis with a spatial resolution of 150 km and an accuracy of 0.2 practical salinity unit (psu) [*Lagerloef et al.*, 2008]. Even in the open ocean (i.e., away from contamination by land), this is a challenging measurement corresponding to a radiometric accuracy on the order of 0.1 K [*Le Vine et al.*, 2010]. Furthermore, at L band, there are competing signals such as radiation from the Sun and radio sources in celestial space that must be identified and removed, and changes in polarization of the desired signal as it traverses the ionosphere (Faraday rotation) that must be corrected. To address these issues, Aquarius has a number of special features. These include the following [*Le Vine et al.*, 2007]: (a) a scatterometer that looks at the same footprint as the radiometers to help provide a correction for roughness (waves), (b) a polarimetric radiometer channel (third Stokes parameter) to correct for Faraday rotation, (c) rapid sampling to help with the detection and mitigation of radio frequency interference (RFI), (d) careful thermal design consisting of active and passive control, and (e) design and orientation of the antennas to avoid radiation from the Sun.

Aquarius is the primary instrument on the Aquarius/SAC-D observatory, a partnership between the USA National Air and Space Agency, NASA, and the Argentine Space Agency, Comisión Nacional de Actividades Espaciales (CONAE). The Aquarius/SAC-D observatory was launched on 10 June 2011 from Vandenberg Air Force Base, California, USA. Aquarius was turned on in late August and the first salinity map was released in September 2011 [see *First Image*, 2011], and Aquarius has been producing maps of the global sea surface salinity field continuously since then. The design and special features of the instrument are contributing to a successful mission. They are also producing new results in their own right with the potential to further enhance understanding of remote sensing from space at L band. The purpose of this article is to provide a brief overview of the status of Aquarius including the instrument and calibration (section 3) and then to present some examples (section 4) with a focus on some of the special features of the Aquarius instrument.

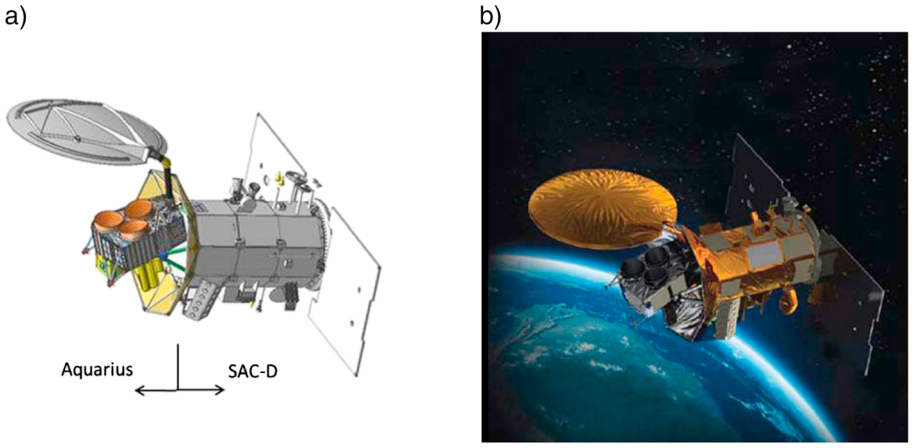

Figure 1. (a) The Aquarius/SAC-D observatory in its deployed configuration. (b) How Aquarius might look in space.

2. Aquarius/SAC-D Observatory

Figure 1a is a drawing showing the observatory in its deployed configuration, and Figure 1b is an illustration showing how it might look in space. Aquarius is the large structure at the end (left) of the spacecraft bus (Figure 1a). It is separated from the SAC-D "bus" by a large umbrella shaped structure which is part of the thermal control of the instrument (a Sun shield). The solar arrays are at the opposite end of the bus. The observatory flies out of the paper toward the reader with the long axis of the bus aligned perpendicular to the velocity vector.

Aquarius consists of three L band radiometers (1.41 GHz) and an L band scatterometer (1.26 GHz). The feeds of the three radiometers with the antenna reflector in the deployed configuration are visible in Figure 1. The projected aperture of the reflector is 2.5 m in diameter which produces radiometer antenna beams about 6.5° wide (full width) at the 3 db point. The radiometers measure vertical and horizontal polarizations and the third Stokes parameter. The third Stokes parameter is obtained by also detecting the sum and difference of the two polarizations (i.e., $V \pm H$) and then taking the difference of the detected signals.

The radiometer beams look to the side (left and in the plane of the figure) and image in push broom fashion. This is illustrated in Figure 2 which shows the ground track and the three radiometer beam footprints. The three beams are oriented approximately perpendicular to the ground track and together cover a swath of 390 km [*Le Vine et al*., 2007]. The incidence angles at the ground of the beam centers are 29.2°, 38.4°, and 46.3° for innermost, middle, and outermost beams, respectively. These angles differ slightly from the nominal prelaunch values of 28.7°, 37.8°, and 45.6° and are the result of a postlaunch assessment of the true pointing.

The instrument contains three separate radiometers, one for each feed. The front end electronics is mounted on the Orthomode Transducer (OMT) behind the feed (e.g., see Figure 5 in *Le Vine et al*. [2007]). However, there is one scatterometer which cycles among the three radiometers. The scatterometer and radiometers share the same feed horns and are designed to look at approximately the same footprint at the same time (see *Le Vine et al*. [2007] for a timing diagram). The scatterometer measures HH, HV, VH, and VV, but only the amplitude (i.e., it is not coherent). The radiometer is the primary instrument for measuring salinity. The scatterometer is present to help with the correction for surface roughness (waves) which is among the most significant potential sources of error [*Dinnat et al*., 2003; *Font et al*., 2004; *Yueh et al*., 2001]. The correction for changes in emissivity caused by roughness can be almost as large as the salinity signal itself.

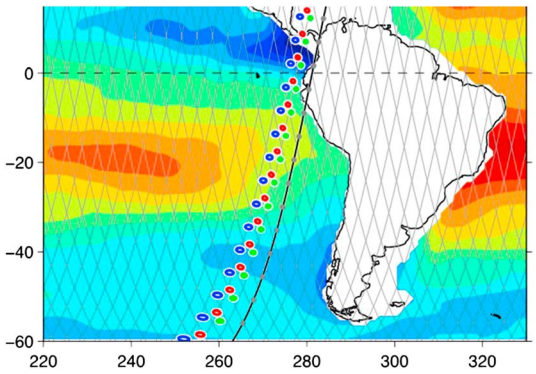

Figure 2. Aquarius ground tracks. The track highlighted is a descending track and shows the footprint of the three radiometers (colored circles).

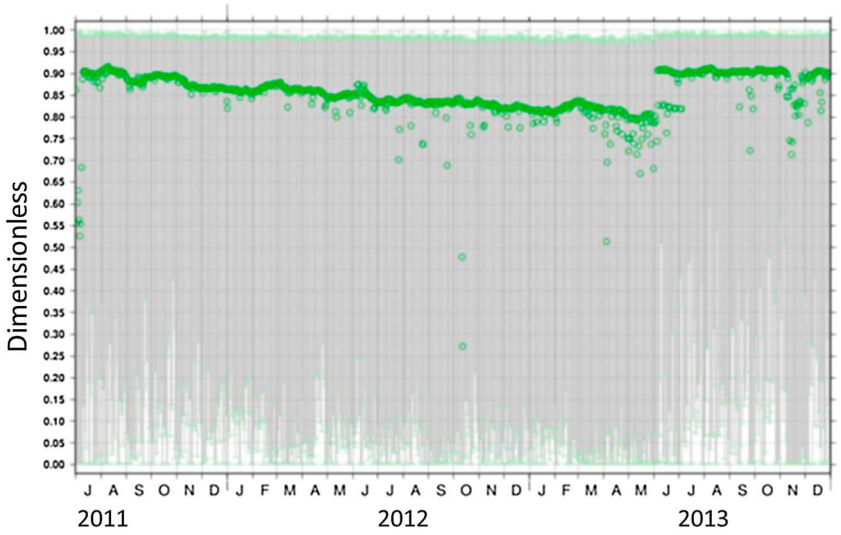

Figure 3. Graph of the quality index of the Aquarius star tracker. Gray indicates the orbital values, and green is the weekly average.

The observatory flies in a Sun-synchronous orbit with a 6:00 P.M. (ascending) equatorial crossing time and is oriented so that the radiometer beams are looking away from the Sun toward the nighttime side of the orbit. In Figures 1 and 2 the Sun is to the right (behind the solar panels in Figure 1). This configuration helps to minimize reflected (backscattered) solar radiation at L band entering the main lobes of the antenna. Solar radiation can also enter via the direct ray from the Sun and a ray reflected from the surface to the right. Attention was given in the antenna design to minimize the side lobes in these directions.

The Argentine Space Agency, CONAE, contributed the spacecraft bus and several instruments. The CONAE portion of the observatory is separated from Aquarius by the umbrella-like Sun shield in Figure 1. The CONAE contribution is called "SAC-D" which is an abbreviation for Satelite de Aplicaciones Cientificas (SAC), and the "D" indicates the fourth in this partnership with the United States. Among the instruments on SAC-D are a Microwave Radiometer (MWR) which operates at 36.5 GHz and 23.8 GHz [*Biswas et al.*, 2012]. The MWR is at the bottom right in Figure 1 (closest to the solar panel) and consists of two pairs of radiometers looking forward and aft of the spacecraft. Each pair is a multibeam (eight beams), push broom radiometer whose field of view is designed to coincide with that of Aquarius. Research is underway among the Aquarius team to incorporate MWR data into the salinity retrieval in the form of a rain flag. Other instruments on the bus include infrared and visible cameras for studying forest fires and light pollution, and a data collection system. In addition, a radio occultation experiment called Radio Occultation for Sounding of the Atmosphere (ROSA) was contributed by the Italian Space Agency, and a space particle detection experiment called Environment Characterization and Modeling (CARMEN) was contributed by the French Space Agency [*Le Vine et al.*, 2007]. Recent papers describing the status and examples of data from these instruments were presented at the Aquarius/SAC-D Science Team meeting in Buenos Aires in November 2013 and are available at the meeting website: http://www.conae.gov.ar/prensa/Eventos/dia1.html.

3. Instrument Status

Aquarius was turned on in late August 2011, and the first salinity map was released 1 month later in September [see *First Image*, 2011]. Aquarius and the Aquarius/SAC-D have been performing well with only minor issues.

3.1. Spacecraft Bus

One issue that caused concern soon after launch was noise in the star tracker. In addition to being noisier than anticipated, the performance metric for the device showed a trend downward with time (i.e., things were getting worse). This is illustrated in Figure 3 which shows the star tracker metric (a relative number between 0 and 1, with 1.0 being best) as a function of time from the beginning of the mission. Among the

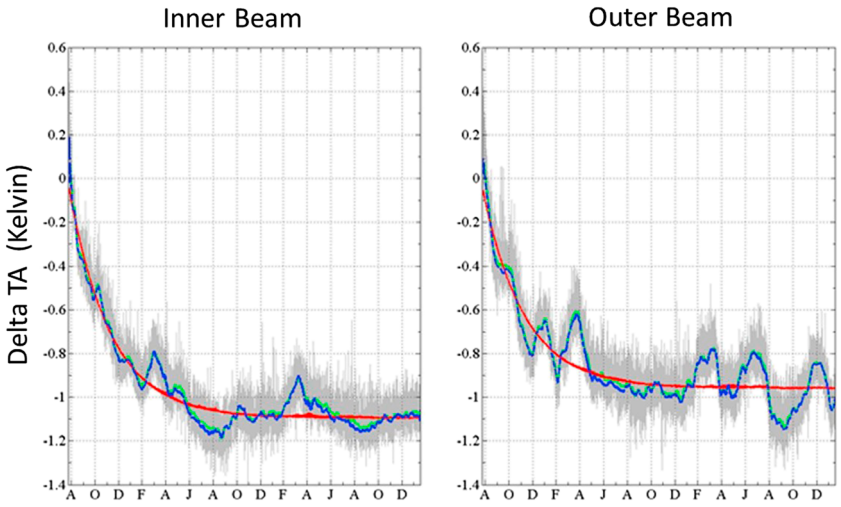

Figure 4. The difference between actual and expected antenna temperature. Gray shows the orbital values, and green is the weekly average. Red is an exponential fit to the data. Results are shown from the beginning of the mission (August 2011) until February 2014. The data on the left are for the inner beam (V-pol), and the data on the right are for the outer beam (V-pol).

consequences of this poor performance was a false signal when the Moon got close to the field of view which sent the spacecraft into safe-hold mode. Eventually, this behavior was traced to noise in the detector CCD array, and by reducing the operating temperature of the array and making software adjustments in the attitude control system, this problem was essentially eliminated. The effect of the reduced operating point can be seen in the large jump near the end of the record. The performance has been stable since (the disturbance very near the end of the record is due to testing).

The other noteworthy issue to report since launch was the failure of a redundant "switch" in the power distribution path. Power is delivered to the instruments in three groups. Each group is fed from the main power supply through a redundant switch and DC-to-DC converter. One of these redundant paths failed. The parallel path was designed to take over the full load if its redundant partner failed, and it did so in this case. There was no impact to the spacecraft. The subsequent engineering analysis suggested that this was a random event, and that there was no reason to believe that the existing path is any more likely to fail than before. The net effect appears to be that redundancy has been lost in one path.

Also, at the time of the final review of this manuscript, undiagnosed anomalies in the housekeeping data from the MWR have resulted in it being turned off. Engineering analysis of the problem is underway.

3.2. Aquarius Radiometers

The Aquarius radiometers have performed very well. The thermal control of the radiometer front ends has been within the requirement (a change of less than 0.1°C per orbit), and the radiometer performance was close to that predicted using an L band computer "simulator" developed prelaunch to study the expected antenna temperature. (The expected value is a theoretical prediction using a numerical simulator which propagates the signal from a reference ocean to the spacecraft [*Le Vine et al.*, 2011b].) However, over time it became clear that a small drift in gain has been present since launch.

The radiometer drift is illustrated in Figure 4 which shows the difference between the measured antenna temperature and the expected value. The difference is plotted in Figure 4 from the beginning of the mission (August 2011) for 2.5 years (February 2014). The difference for each orbit is shown in gray, and the 7 day average is shown in green. The red curve is an exponential fit. The drift appears to have an exponential shape as a function of time with small variations about the mean exponential which in Aquarius circles have been dubbed "wiggles." Although the drift is small (about 1 K the first year) and appears to be flattening, it is noticeable in the salinity maps, for example, when looking at long-term (e.g., interannual) variations in the global salinity field.

The drift is currently being removed as part of the radiometer calibration. (Calibration involves two parts, the antenna and the radiometer electronics. The antenna is discussed below in section 3.3, and the following

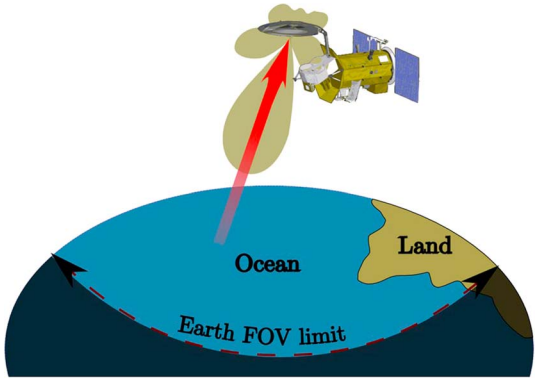

Figure 5. Remote sensing from space. The Aquarius Earth viewing geometry.

discussion outlines how the drift is taken into account as part of the calibration of the radiometer electronics. Details can be found in *Wentz and Le Vine* [2012]. Correcting for drift is a two-step process in which the mean behavior is removed by fitting an exponential to the mission history (e.g., the red curve in Figure 4). The change represented by the exponential is treated as a gain drift and removed by adjusting the value of the noise diode in the calibration equations [*Piepmeier et al*., 2013]. Then, a weekly running mean of the remaining difference between the measured and the expected values of antenna temperature is used to remove the wiggles (which are treated as an offset). A root cause for the drift is a subject of investigation. Outgassing was initially suggested as a possibility for the exponential behavior, and the radiometer backend electronics has been proposed as a source of the wiggles. Nothing is confirmed at this point; however, progress is being made and it is hoped to eventually have a calibration that relies only on hardware and not on the salinity measurements.

3.3. Algorithm

There have also been a couple of issues associated with the salinity retrieval algorithm that have been identified and led to improvements in the retrieved salinity. One of these is a difference that was noticed in the salinity retrievals over the same ocean obtained when using only ascending orbits as opposed to only descending orbits. Since the retrievals were over the same ocean, they should have yielded the same salinity. This difference has been traced to the celestial background radiation. This can be an important signal when reflected from the surface and picked up by the radiometer main beam. The contribution varies seasonally and is strongest when the plane of the galaxy is overhead [*Le Vine and Abraham*, 2004; *Dinnat et al*., 2008]. The problem appears to be inadequacy of the physical optics scattering theory used in the analysis [*Wentz and Le Vine*, 2012] to correct completely for the effect of roughness (waves). An empirical correction has been developed which tunes the existing correction and removes the "bias." This correction will be implemented in the new version of the data product, V3.0, which was released in June 2014 [*Wentz and Le Vine*, 2012, Addendum III] (also see section 5 below).

Another algorithm issue has been the impact of uncertainties associated with the antenna pattern on the radiometer calibration. This is illustrated in equations (1a) and (1b), which are the traditional expressions for the response of an antenna with gain, G, with an input brightness temperature, Tb [*Ulaby and Long*, 2014]:

$$\mathrm{TA} = (1/4\pi) \int \mathrm{Tb}(\Omega)\, G(\Omega)\, \mathrm{d}\Omega \tag{1a}$$

$$= (1/4\pi) \int_{\mathrm{Earth}} \mathrm{Tb}(\Omega)\, G(\Omega)\, \mathrm{d}\Omega + (1/4\pi) \int_{\mathrm{sky}} \mathrm{Tb}(\Omega)\, G(\Omega)\, \mathrm{d}\Omega \tag{1b}$$

In equation (1b), the integral is divided into two parts, an integral over the visible disk as seen by the sensor and designated "Earth," and the remainder designated "sky." The geometry for a sensor in space looking down on the Earth is as shown in Figure 5. The Earth portion of the integral (the portion of the Earth visible from space and defined by the dashed line) includes the desired signal and is dominated by the antenna main beam. The sky portion receives signal originating off the Earth. The signal is mostly "cold sky" and the Sun which are viewed through the antenna side lobes. In the Aquarius salinity retrieval, the sky portion is computed using models for the sky and antenna and removed [*Wentz and Le Vine*, 2012]. Then, the remaining integral is solved for the desired brightness temperature using a semiempirical approach in which it is reduced to a matrix equation (see Antenna Pattern Correction in *Wentz and Le Vine* [2012]).

Suppose an error is made in the antenna pattern and too little power is assigned to the sky portion of the pattern. This will make only a small error in the second integral in (1b) because $\mathrm{Tb}^{\mathrm{sky}}$ is small at L band, and it is weighed by the antenna sidelobes. However, because G is conserved, there will also be an error in the gain appearing in the Earth integral and therefore an error in this integral. It is possible for this error to be hidden

and absorbed in the calibration, especially if the application is only to a fixed point (e.g., the ocean). However, the error will become apparent when applied to scenes with a large range of brightness temperature.

For example, suppose the antenna pattern, *G*, in the Earth integral is smaller than it should be because of an overestimate of the power in the back lobes; and suppose the radiometer operating point (calibration curve) has been adjusted so that the correct TA is obtained when the scene is ocean (Tb about 100 K). This could be done, for example, if the deficit in the output of the antenna (Earth term in equation (1b)) is compensated by adjusting the gain of the radiometer hardware. In this case, the operating curve passes through ocean but does not have the correct slope (a bit high in this case). Hence, the same operating curve used over land (250 K) will produce a retrieved Tb too large (too warm), and when used to look at cold sky (4 K) will produce a signal too small (cold).

This situation occurred with Aquarius. The antenna-feed system was too large to measure on the ground (i.e., prelaunch). Instead, patterns were obtained using a scale model of the spacecraft and two numerical models. All gave reasonably similar main beam patterns but with significant differences in the sidelobes and cross-polarization coupling. The most recent numerical model (which included more of the spacecraft than the original) was adopted in V2.0 of the Aquarius retrieval algorithm for developing the "antenna pattern correction" [*Wentz and Le Vine*, 2012] used in retrieving Tb from the Earth integral in equation (1b). The result worked well over ocean, but when checked over land, there was a clear warm bias and views of cold sky (e.g., when the spacecraft is inverted during the cold sky calibration) were too cold [*Dinnat et al*., 2014].

Research is underway to correct this problem. Measurements of the sky fraction of the antenna pattern have been made by inverting the spacecraft and flying over well-characterized land-water transitions; and adjustments to the antenna pattern correction [*Wentz and Le Vine*, 2012, Addendum III] have improved the response at the warm end significantly. Recent checks over reference sites, such as the DOME-C in Antarctica and the U.S. Department of Agriculture watersheds at Little River and Little Washita in the U.S., have shown a significant reduction in the warm bias [*Dinnat et al*., 2014]. Version 3.0 includes the improved full-range calibration [*Wentz and Le Vine*, 2012, Addendum III].

4. Examples

4.1. Aquarius Data Products

4.1.1. Sea Surface Salinity

Aquarius maps the globe once each week (7 day exact repeat orbit). The orbital data are updated monthly, and the salinity data products are available to the public from the NASA Physical Oceanography Distributed Active Archive Center (DAAC) at http://podaac.jpl.nasa.gov/aquarius. This site also includes user guides and other relevant documentation (e.g., the Algorithm Theoretical Basis Document for the radiometer and scatterometer). An exact repeat orbit was chosen for Aquarius to facilitate averaging which is part of the strategy to achieve the desired accuracy of 0.2 psu. An exact repeat orbit has the advantage for this purpose that the same locations on the Earth are viewed the same way every repeat cycle (i.e., 7 days). The beam resolution and swath were chosen to give global coverage with only very small gaps (10 km) at the equator.

4.1.2. Soil Moisture

Aquarius is now also producing a soil moisture product which is available from the National Snow and Ice Data Center: www.nsidc.org/data/aquarius/index.html. The procedure for transferring from antenna temperature to brightness temperature at the surface is the same over ocean and land; however, instead of correcting for wave roughness and retrieving salinity, the surface TB over land is processed to retrieve soil moisture. A single-channel algorithm using horizontal polarization is employed [*Bindlish and Jackson*, 2013].

4.1.3. Background

Examples of the data products, such as salinity, soil moisture maps, and plots of radiometer and scatterometer RFI, are available at the Aquarius education and public outreach website at www.aquarius.umaine.edu. This site also includes background and historical information and links to the data and to other sources of information about Aquarius.

4.2. Sea Surface Salinity

The primary goal of Aquarius is to map the features of the global surface salinity field in the open ocean. Figure 6 is an example. The image on the left shows the global surface salinity field retrieved by Aquarius

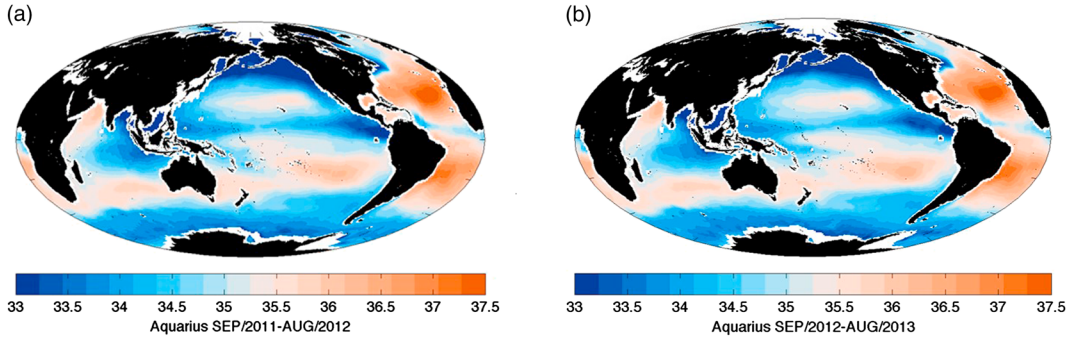

Figure 6. Aquarius salinity maps. (a) On the left is the global average salinity field obtained during the first year of Aquarius observations (September 2011 to August 2012). (b) On the right is the global average salinity field obtained during the second year of Aquarius observations, September 2012 to August 2013.

averaged for 1 year from September 2011 through August 2012. The map is constructed by regridding the Level 2 data to a resolution of 1° in latitude and longitude and averaging over 1 year of operations. The map on the right shows the data for the second year of Aquarius operation, September 2012 through August 2013. The maps reveal expected features of the surface salinity field, such as higher average salinity in the Atlantic Ocean compared to the Pacific Ocean and the relatively fresh belt near the equator associated with the higher frequency of rain in the Intertropical Convergence Zone. These features reflect the large-scale structure associated with patterns of rainfall and evaporation over the ocean as modified by ocean circulation. Other important regional features are also evident, including the sharp contrast between the high-salinity Arabian Sea west of the Indian subcontinent where evaporation is dominant and the low-salinity Bay of Bengal to the east which is dominated by the Ganges River outflow and rains of the South Asia monsoon.

Salinity maps are produced weekly and monthly. The monthly maps also show many dynamic features of the salinity field such as the evolution of the freshwater plume from large river systems such as the Amazon River. Changes in the salinity of the Indian Ocean in the Bay of Bengal associated with the ebb and flow of the monsoon can also be seen in these images. Animations illustrating the dynamics of the salinity field such as these are available at the public outreach site: http://www.aquarius.umaine.edu (e.g., look under "gallery").

One of the goals of Aquarius is to study the long-term changes in the mean salinity field. Figure 7 presents an example. This is the difference between the mean salinity field during Aquarius' first year of operation (Figure 6a) and the second year (Figure 6b). Some features stand out, such as the fresh band in southern Pacific Ocean extending from Indonesia south eastward almost to South America. Also, there are striking saline features on the East and West Coast at the tip of South America. More data are needed to understand the significance of such features, but the clear evidence of changes seen in Figure 7 is one of the ways Aquarius is contributing to better understanding of the global salinity field.

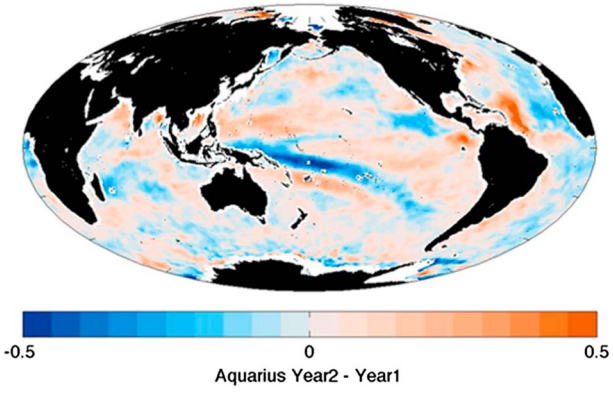

Figure 7. The difference between the mean global salinity field obtained by Aquarius during its first 2 years of operation.

The measurement goal of Aquarius is a root-mean-square accuracy on a global basis of 0.2 psu [*Le Vine et al.*, 2007; *Lagerloef et al.*, 2008]. The Aquarius Validation Data System (AVDS) was established to help validate the performance of the Aquarius retrieval against this goal [*Aquarius Validation Data System*, 2014]. This is a data base in which in situ salinity measurements from buoys and Argo profiling floats are matched to Aquarius footprints in time and space. Figure 8 is an example, reporting histograms for the three beams of the difference between the in situ salinity and salinity retrieved by Aquarius. The mean

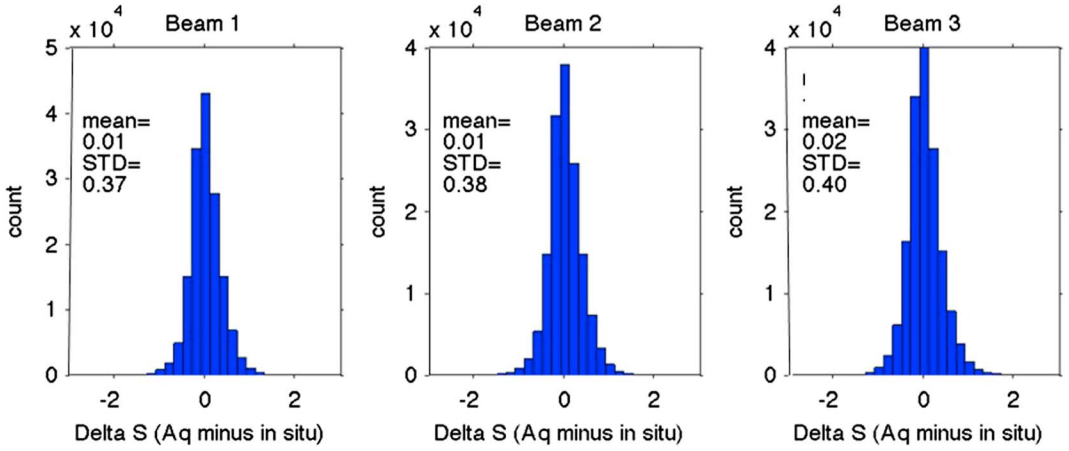

Figure 8. Histograms of the difference between Aquarius salinity and in situ salinity.

difference is quite small but the standard deviation of the difference is on the order of 0.4 psu (0.37, 0.38, and 0.40 for the three beams, respectively). While this exceeds the goal, it also reflects the error in both the Aquarius retrievals and also those in the in situ measurements. One technique for separating the error is "triple location" (i.e., given three independent measurements with independent error, it is possible to solve for the error of each one independently). One choice for the three measurements is: (a) the Aquarius measurements; (b) the value from the colocated Argo floats; and (c) the surface salinity from the HYCOM ocean model [*Chassignet et al*., 2007]. Using this set leads to an error estimate for Aquarius by itself on the order of 0.25 psu. These sources are not completely independent (e.g., the HYCOM model ingests Argo measurements), but the number suggest that Aquarius is nearing its goal. Most importantly, the error estimates continue to decrease as improvements are made in the retrieval algorithm.

4.3. Aquarius Special Features

The special features of the Aquarius instrument which have been designed to help produce an accurate map of the global salinity field also produce independent data of their own. Below are several examples of the additional information coming from Aquarius as a result of these features of the instrument.

4.3.1. RFI Maps

One of the special features of Aquarius is the provision for rapid sampling which was included to facilitate the detection and mitigation of manmade radio frequency interference (RFI). The rapid sampling is used with a "glitch" detection algorithm [*Ruf and Misra*, 2008] designed to detect RFI from pulsed sources such as radar which are a known problem at L band [*Niamsuwan and Johnson*, 2005]. This has been working well [*Le Vine et al*., 2014]. One of the other unique features of Aquarius is the nearly simultaneous look with both active and passive sensors at the same scene. Taken together these two features allow Aquarius to map RFI as seen by both the radiometer and scatterometer over the same scene. This is of increasing importance as new sensor technologies emerge using combined active/passive measurements to improve the remote sensing product (e.g., the Soil Moisture Active Passive (SMAP) instrument which combines active and passive observations to improve the spatial resolution in the retrieval of soil moisture [*Entakhabi et al*., 2010]).

Figure 9 is an example. The top panels show the frequency of occurrence of RFI as detected by the scatterometer (Figure 9, left) and radiometer (Figure 9, right). The detection algorithms and characteristics of the RFI maps are described in *Le Vine et al*. [2014] and *Le Vine and de Matthaeis* [2014], respectively. A disappointing surprise is the large extent of radiometer RFI over continental Europe and Asia even though the radiometers operate in a protected band where emissions are prohibited. The bottom panels are an expanded view of the panels on top showing the continental U.S. in more detail. The figure on the bottom right shows the detected RFI in the radiometer band (1.41 GHz). It is clear that the U.S. is relatively free of RFI in this band. This is not as true in many areas of the rest of the world even though the protection is international, as is indicated by the red areas in the top panels. The RFI map for the scatterometer (1.26 GHz) in the U.S. is a much different story (bottom, left). The U.S. is almost completely covered by RFI in the scatterometer band. This is not really a surprise because the scatterometer band (1.26 GHz) is shared with

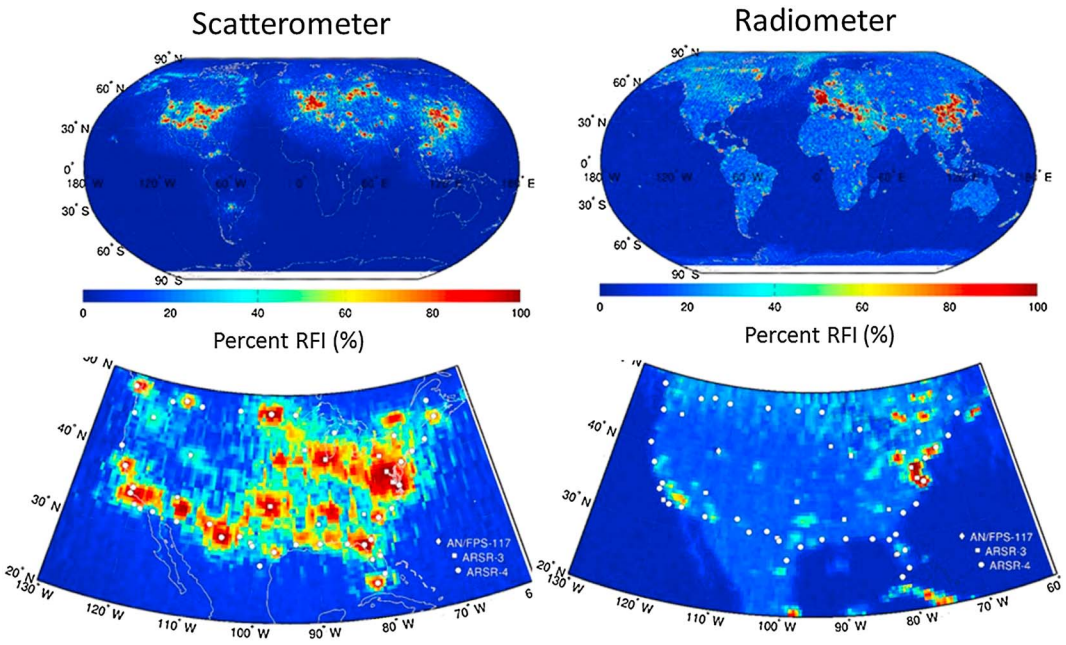

Figure 9. (right) Radiometer and (left) scatterometer RFI. The percentage of samples identified as RFI is plotted for each sensor. The bottom maps show the same data but with an expanded view over the United States.

other users, principally air traffic control radar. To illustrate this, white dots have been added to indicate the location of several types of air traffic control radar that operated in this band. On the right hand side (radiometer), there is little correlation between the areas of high likelihood of RFI (red) and the location of the radar (white dots); but on the left side there is a very strong correlation.

4.3.2. Faraday Rotation

Another special feature of Aquarius is the inclusion of a polarimetric channel to measure the third Stokes parameter. The objective is to provide an in situ, real-time measure of the Faraday rotation of the signal propagating from the surface through the ionosphere to the spacecraft. Faraday rotation is important at L band [*Le Vine and Abraham*, 2002] and particularly important for remote sensing of salinity which has a relatively small dynamic range (e.g., compared to soil moisture). The approach is to use the ratio of the third and second Stokes parameter, as outlined by *Yueh* [2000]. This plan has worked well [*Le Vine et al*., 2013]. Not only have accurate values of Faraday rotation have been retrieved [*Le Vine et al*., 2013], but the third Stokes parameter exhibited the behavior (smooth over ocean and noisy over land) predicted by theory [*Le Vine et al*., 2011a].

Figure 10 is an example. It shows a comparison of the Faraday rotation retrieved by Aquarius and retrieved using the total electron content (TEC) measured by the altimeter on the Jason-2 spacecraft [*Bannoura et al*.,

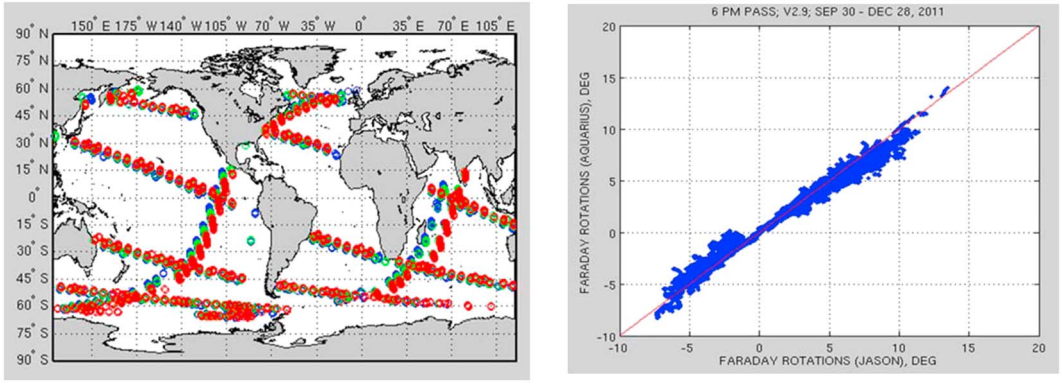

Figure 10. Comparison of Faraday rotation retrieved by Aquarius and the Jason altimeter. The map on the left shows the location of the intersections of the two sensors, and the comparison of the retrieved Faraday rotation is shown on the right.

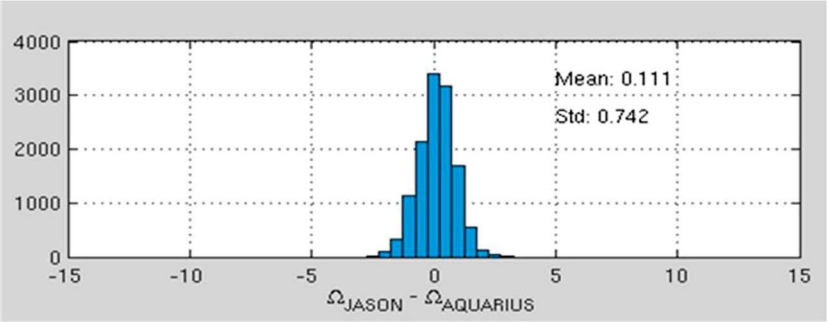

Figure 11. Histogram of the difference between Faraday rotation angle retrieve by Aquarius and from the Jason-2 altimeter.

2005] at points where the two spacecraft intersect. (The TEC from the altimeter is used with the local geomagnetic field to compute the Faraday rotation expected from the Aquarius radiometer.) Coincidence is declared if the two spacecraft are within 30 min and with a circle of 0.5° relative to the Aquarius boresight. The figure on the left shows the locations of the intersections. The colors indicate the three Aquarius radiometer beams (blue for the inner beam, green for the middle beam, and red for the outer beam). The figure on the right shows the comparison between the Faraday rotation angle retrieved by Aquarius (ordinate) and that retrieved from the Jason-2 TEC (abscissa). All of the values from Jason-2 within the box of intersection are averaged to reduce noise. A few cases, one where Aquarius appears to be affected by land and five where Jason-2 appears to affected by ice, have been eliminated (out of a total of more than 150). Otherwise the two retrievals agree well. They also agree well with the value predicted using the TEC maps produced by the International Global Navigation Satellite Systems Service [*Le Vine et al*., 2013]. There is a slight bias in the comparison (about 0.1°). This is shown more clearly in Figure 11, which is a histogram of the differences between the Faraday rotation angle retrieved by Aquarius and from the Jason-2 altimeter TEC. Some of this bias could be due to the calibration of the Aquarius radiometers. The comparison has improved as the antenna pattern correction used in the algorithm has been updated (e.g., see the discussion in section 3.3 above). The comparison shown in Figures 10 and 11 has been obtained using the most up-to-date antenna pattern correction. This is the version used in V3.0 of the retrieval algorithm released in June 2014.

4.3.3. Other

In addition to the examples presented above, data from Aquarius are being used for other novel applications. As mentioned above, a soil moisture product is available [*Bindlish and Jackson*, 2013]. In addition, the active/passive data have been used to verify the effects of topography on the brightness temperature observed by an L band radiometer [*Utku and Le Vine*, 2014], and new applications are being developed to study the cryosphere [*de Matthaeis et al*., 2014; *Brucker et al*., 2014a, 2014b, 2014c]. Data specific to the cryosphere are available at http://nsidc.org/data/aquarius/index.html.

Also, in addition to being critical for the correction for roughness, the presence of the scatterometer has permitted estimates of wind speed over the ocean with results that agree well with other satellite measurements [*Yueh et al*., 2013; *Fore et al*., 2013]. In addition, the combination of the scatterometer and the MWR is leading to new insight into the effect of rain on the radiometer signal and on remote sensing of sea surface salinity [*Tang et al*., 2013].

5. Mission Status

Aquarius is doing well. The hardware has been functioning well with only minor issues, and Aquarius is producing salinity maps with a promise of new insight into the salinity field. In addition, the special features such as active/passive combination, rapid sampling, and a polarimetric channel are also generating new information.

An improved salinity product was released in June 2014. Version 3.0 has a number of improvements, including an improved antenna pattern correction and associated full-range calibration (e.g., section 3.3) and an improved correction for the ascending/descending bias associated with the reflected signal from the galaxy. It also uses data at both polarizations, vertical and horizontal, in the retrieval whereas the earlier

version used only vertical polarization. Data and associated documentation are available to the public at the Physical Oceanography Distributed Active Archive Center: http://podaac.jpl.nasa.gov/aquarius.

The Aquarius prime mission ends at the end of November 2014 (e.g., 3 years of operations following completion of commissioning). However, the mission has been extended to the end of September 2015 (end of the government fiscal year) to align its schedule with other NASA missions. Assuming all is working well and new science continues to be produced, a proposal will be made by the project team to extend Aquarius for two more years (October 2015 to September 2017). In addition to providing a longer record of salinity maps, an extension will provide a period of overlap with SMAP and the Soil Moisture Ocean Salinity (SMOS) mission [*Kerr et al*., 2010].

If all goes well, the remote sensing community could soon have three L band sensors in space at the same time, Aquarius, SMOS, and SMAP. Although each sensor produces radiometric observations at 1.413 GHz (L band) with applications to soil moisture and ocean salinity, each brings something unique and breaks new ground in remote sensing. Aquarius has just been described. It is active/passive, polarimetric and includes, possibly, the most accurate L band radiometer ever to operate in space. SMOS is unique, demonstrating a new technology, interferometric radiometry [*Martin-Neira et al*., 2014], which could lead the way for radiometers with high spatial resolution in the future. SMAP builds on the shoulders of the others and goes a step further. It is active/passive and promises a significant improvement in spatial resolution and protection from RFI [*Piepmeier et al*., 2014]. This is truly the golden age of L band remote sensing from space.

Acknowledgments
Data and associated documentation are available to the public at the physical oceanography DAAC: http://podaac.jpl.nasa.gov/aquarius.

References

Aquarius Validation Data System (2014), Aquarius Validation Data System. [Available at https://aquarius.esr.org/avds/.]
Bannoura, W. J., A. Wade, and D. N. Srinivas (2005), NOAA ocean surface topography mission Jason-2 project overview, *Proc MTS/IEEE Oceans*, *3*, 2155–2159.
Bindlish, R., and T. Jackson (2013), Soil moisture product using Aquarius/SAC-D observations, V2.0, Aquarius Soil Moisture ATBD Users Guide, Version 2.0. [Available at http://nsidc.org/data/docs/daac/aquarius/pdfs/Aquarius_VSM_ATBD_UsersGuide.pdf.]
Biswas, S. K., L. Jones, D. Rocca, and J.-C. Gallio (2012), Aquarius/SAC-D Microwave Radiometer (MWR): Instrument description & brightness temperature calibration, Geoscience and Remote Sensing Symposium (IGARSS), IEEE International, doi:10.1109/IGARSS.2012.6350705.
Brucker, L., E. P. Dinnat, G. Picard, and N. Champollion (2014a), Effect of snow surface metamorphism on Aquarius L-band radiometer observations at Dome C, Antarctica, *IEEE Trans. Geosci. Remote Sens.*, *52*(11), 7408–7411.
Brucker, L., E. P. Dinnat, and L. Koenig (2014b), Weekly-gridded Aquarius L-band radiometer/scatterometer observations and salinity retrievals over the polar regions—Part 1: Product description, *The Cryosphere*, *8*(3), 905–913.
Brucker, L., E. P. Dinnat, and L. Koenig (2014c), Weekly-gridded Aquarius L-band radiometer/scatterometer observations and salinity retrievals over the polar regions—Part 2: Initial product analysis, *The Cryosphere*, *8*(3), 915–930.
Chassignet, E. P., et al. (2007), The HYCOM (HYbrid Coordinate Ocean Model) data assimilative system, *J. Mar. Syst.*, *65*(1–4), 60–83. [Available at http://hycom.org/dataserver.]
de Matthaeis, P., C. Utku, D. M. Le Vine, and A. Moyer (2014), Aquarius retrieval of sea ice thickness: Initial results, Microwave Radiometry and Remote Sensing of the Environment (MicroRad), 13th Specialist Meeting on, pp 69–71, Pasadena, Calif., March, doi:10.1109/MicroRad.2014.6878910.
Dinnat, E. P., J. Boutin, G. Caudal, and J. Etcheto (2003), Issues concerning the sea emissivity modeling at L-band for retrieving surface salinity, *Radio Sci.*, *38*(4), 8060, doi:10.1029/2002RS002637.
Dinnat, E. P., D. M. Le Vine, and S. Abraham (2008), L-band radiometry and reflection of the galaxy by a rough ocean surface, Microwave Radiometry and Remote Sensing of the Environment (MicroRad), 13th Specialist Meeting on, pp. 1–4, Firenze, Italy, doi:10.1109/MICRAD.2008.4579494.
Dinnat, E. P., D. Le Vine, R. Bindlish, and J. Piepmeier (2014), Aquarius whole range calibration: Celestial sky, ocean, and land targets, in *Microwave Radiometry and Remote Sensing of the Environment (MicroRad)*, March, Pasadena, Calif.
Entakhabi, D., et al (2010), The Soil Moisture Active Passive (SMAP) mission, *Proc. IEEE*, *98*(5), 704–716.
First image (2011). [Available at http://www.nasa.gov/mission_pages/aquarius/news/aquarius20110922.html#.U0cuJFcmxU8.]
Font, J., G. S. E. Lagerloef, D. M. Le Vine, A. Camps, and O.-Z. Zanife (2004), The determination of surface salinity with the European SMOS space mission, *IEEE Trans. Geosci. Remote Sens.*, *42*(10), 2196–2205.
Fore, A. G., S. H. Yueh, W. Tang, and A. K. Hayashi (2013), Aquarius wind speed products: Algorithms and validation, *IEEE Trans. Geosci. Remote Sens.*, *52*(5), 2920–2927, doi:10.1109/TGRS.2013.2267616.
Kerr, Y. H., et al. (2010), The SMOS mission: New tool for monitoring key elements of the global water 8 cycle, *Proc. IEEE*, *98*(5), 666–687.
Lagerloef, G. S. E., et al (2008), The Aquarius/SAC-D mission: Designed to meet the salinity remote sensing challenge, *Oceanography*, *21*(1), 69–81.
Le Vine, D. M., and S. Abraham (2002), The effect of the ionosphere on remote sensing of sea surface salinity from space: Absorption and emission at L band, *IEEE Trans. Geosci Remote Sens.*, *40*(4), 771–782.
Le Vine, D. M., and S. Abraham (2004), Galactic noise and passive microwave remote sensing from space at L-band, *IEEE Trans. Geosci. Remote Sens.*, *42*(1), 119–129.
Le Vine, D. M., and P. de Matthaeis (2014), Aquarius active/passive RFI environment at L-band, *IEEE Geosci. Remote Sens. Lett.*, *11*(10), doi:10.1109/LGRS.2014.2307794.
Le Vine, D. M., G. S. E. Lagerloef, R. Colomb, S. Yueh, and F. Pellerano (2007), Aquarius: An instrument to monitor sea surface salinity from space, *IEEE Trans. Geosci. Remote Sens.*, *45*(7), 2040–2050.
Le Vine, D. M., G. S. E. Lageroef, and S. E. Torrusio (2010), Aquarius and remote sensing of sea surface salinity from space, *IEEE Proc.*, *98*(5), 688–703.
Le Vine, D. M., E. P. Dinat, S. D. Jacob, S. Abraham, and P. de Matthaeis (2011a), Impact of Antenna pattern on measurement of the third Stokes parameter from space at L-band, *IEEE Trans. Geosci. Remote Sens.*, *49*(1), 406–414.

Le Vine, D. M., E. P. Dinnat, S. Abraham, P. de Matthaeis, and F. J. Wentz (2011b), The Aquarius simulator and cold-sky calibration, *IEEE Trans. Geosci. Remote Sens.*, *49*(9), 3198–3210.

Le Vine, D. M., S. Abraham, C. Utku, and E. P. Dinnat (2013), Aquarius third Stokes parameter measurements: Initial results, *IEEE Geosci. Remote Sens. Lett.*, *10*(3), 520–524.

Le Vine, D. M., P. de Matthaeis, C. Ruf, and D. Chen (2014), Aquarius RFI detection and mitigation algorithm: Assessment and examples, *IEEE Trans. Geosci. Remote Sens.*, *52*(8), 4574–4584.

Martin-Neira, M., et al (2014), Microwave interferometric radiometry in remote sensing: An invited historical review, *Radio Sci.*, *49*, 415–449, doi:10.1002/2013RS005230.

Niamsuwan, N., and J. T. Johnson (2005), Examination of a simple pulse-blanking technique for radio frequency interference mitigation, *Radio Sci.*, *40*, RS5S03, doi:10.1029/2004RS003155.

Piepmeier, J. R., et al. (2014), Radio-frequency interference mitigation for the soil moisture active passive microwave radiometer, *IEEE Trans. Geosci. Remote Sens.*, *52* part 2, 761–775, doi:10.1109/TGRS2013.2281266.

Piepmeier, J., et al. (2013), Aquarius radiometer post-launch calibration for product version 2, Aquarius Project Document AQ-014-0015, February. [Available at http://po.daac.jpl.nasa.gov/aquarius.]

Ruf, C., and S. Misra (2008), Detection of radio-frequency interference for the Aquarius radiometer, *IEEE Trans. Geosci Remote Sens.*, *46*(10), 3123–3128.

Tang, W., S. Yueh, A. Fore, G. Neumann, A. Hayashi, and G. Lagerloef (2013), The rain effect on Aquarius' L-band sea surface brightness temperature and radar backscatter, *Remote Sens. Environ.*, *137*, 147–157.

Ulaby, F., and D. Long (2014), *Microwave Radar and Radiometric Remote Sensing*, Section 6.4, The University of Michigan Press, Ann Arbor, Mich.

Utku, C., and D. M. Le Vine (2014), Topographic signatures in Aquarius radiometer and scatterometer response, *IEEE Trans. Geosci. Remote Sens.*, *46*(10), 3123–3128.

Wentz, F. J., and D. M. Le Vine (2012), Version 2: Algorithm theoretical basis document: Aquarius salinity retrieval algorithm, RSS Tech. Rep., 082912 and Aquarius document AQ-014-PS-0017. Also see Addendum I, II and III. [Available at http://jpl.podaac.nasa.gov.]

Yueh, S. H. (2000), Estimates of Faraday rotation with passive microwave polarimetry for microwave remote sensing of Earth surfaces, *IEEE Trans. Geosci. Remote Sens.*, *38*(5), 2434–2438.

Yueh, S. H., R. West, W. J. Wilson, F. K. Li, E. G. Njoku, and Y. Rahmat-Samii (2001), Error Sources and feasibility for microwave remote sensing of ocean surface salinity, *IEEE Trans. Geosci. Remote Sens.*, *39*(5), 1049–1060, doi:10.1109/36.921423.

Yueh, S. H., W. Tang, A. Fore, G. Neumann, A. Hayashi, A. Freedman, J. Chaubell, and G. Lagerloef (2013), L-band passive and active microwave geophysical model functions of ocean surface winds and applications to Aquarius retrieval, *IEEE Trans. Geosci. Remote Sens.*, *51*(9), 4619–4632, doi:10.1109/TGRS.2013.2266915.